Hydrothermal Synthesis and Characterization of One-dimensional Ceria Nanorod for Chromium Ion Removal from Wastewater

Sujan Chowdhury[1,2*], Madiha Yasir[1], Mohammad Azmi B Bustam[1], Kuen-Song Lin[2]

1. Department of Chemical Engineering, Universiti Teknologi PETRONAS, Bandar Seri Iskandar, 31750 Tronoh, Perak, Malaysia;

2. Department of Chemical Engineering & Materials Sciences, Yuan Ze University, Taiwan R.O.C.;

*Email address of corresponding author: sujan.chowdhury@petronas.com.my

Abstract

Remediation of wastewater contaminated with Cr(VI) species by ceria particles has received considerable attention in recent years. The main objectives of the present study were to investigate the adsorption of Cr(VI) species on the one-dimensional (1-D) ceria nanorod (CeNR). In where, CeNR has 20–40 nm in diameter and 200–300 nm in length, as confirmed through FE-SEM and TEM images. Higher surface area of CeNR is insisted to the remediation of Cr(VI)-contaminated wastewaters. This work exemplifies the utilization of XAS and BET to reveal the speciation of CeNR for further understands of the very complex adsorption process. It is also very clear that decontamination of Cr species in wastewater via the *in-situ* remediation with CeNR permeable reactive barriers would be environmentally attractive in the near future.

Keywords: Cr(VI)-contaminant, One-dimensional Ceria, Wastewater treatment; XANES/EXAFS.

1. Introduction

Growing pollution of the environment has led to intensive investigations into the immobilization or removal of toxic substances from groundwater or waste streams. The interest seeking poisons in waste streams are heavy-metal compounds, and some of them exhibit very hazardous properties. In soils and groundwater, chromium is usually found and appears in the form of Cr(VI) and Cr(III), respectively from the effluent of industrial waste water. In addition, chromium is toxic and considered as possible or probable carcinogens and/or mutagens (Di, 2006; Ponder, 2000; Wang, 2012). Conventional treatments of removing Cr species, such as chemical, biological or membrane separation techniques are costly and non-effective. Reduction of chromium contaminated waste water by oxidation nanoparticle has a great interest. Surface area of oxidation nanoparticle to the aqueous stream, has been shown a promising electron-source material for the *in-situ* remediation of Cr(VI) contaminants in groundwater. It follows that increasing the surface area of the nanophase ceria materials facilitate to increase the remediation of chromium contaminated waste water for economical point of view. General physical and chemical property of the oxidation nanomaterial such like ceria is specifically enhanced through the dimension of the nanostructure with respect to their bulk like materials. The solvent composition and the cerium source are of importance in the final product morphology (Chowdhury, 2011; Lin, 2010). The reaction temperature, concentration of the cerium source, and reaction time has a significant influence on the yield of CeO_2 nanorod (Chowdhury, 2012; Zhang, 2006). The synthesis methods of CeO_2 nanorods were relatively complicated and always needed high-temperature, high-pressure or long-time treatments (Chowdhury, 2012; Chowdhury, 2011; Lin, 2010; Qi, 2005). Therefore, the formation of 1-D ceria nanorods for chromium contaminated ground waste-water treatment application is still an ultimate challenge for cost-effective considerations. The X-ray absorption spectroscopy (XAS) offers the basic knowledge of understanding the oxidation states and fine structures to a study on the surface reaction of 1-D ceria nanorod. X-ray absorption spectroscopy is an excellent technique for characterizing the valency and local structure of metals in 1-D ceria nanorod with a short-range order. X-ray absorption near edge structure (XANES) spectroscopy provides information of electronic configuration, stereochemistry and the oxidation states while, extended X-ray absorption fine structure (EXAFS) spectroscopy can investigate the information on the atomic arrangement in terms of bond distance, number and kind of near neighbors, thermal and static disorder.

Therefore, the main objective of the present study was to investigate the fine structures and oxidation states of 1-D ceria nanorod particles for remediation of Cr contamination in simulated groundwater. The fine structures of catalyst were also identified and characterized using X-ray diffraction (XRD), field-emission-scanning electron microscopy (FE-SEM), Transmission electron microscopy (TEM), EXAFS or XANES techniques.

2. Method

2.1.   Materials and Preparation of Ceria Nanorod

In the typical procedure, $Ce(NO_3)_3 \cdot 6H_2O$ solution (16 mmol, 10 mL) and higher concentration of NaOH solution (14 M, 70 mL) were mixed in a 250 mL capacity Teflon-lined stainless steel autoclave, and left for one day at 100 °C in the digital temperature-controlled oven. The obtained one-dimensional nanorod product was washed with DI water and dried at 60 °C for overnight and calcined at 300 °C for 3h in the presence of flowing air.

2.2.   Characterization and Analysis Techniques

Morphologies, crystallinities, particle size distribution, and the compositions of the commercial ceria powder and as-synthesized 1-D CeNR catalysts were determined by FE–SEM equipped with EDS (Hitachi, S–4700 Type II) and HR-TEM (Zeiss 10C). XRD patterns scanned from 5 to 90°(2θ) with a scan rate of 4°(2θ) min⁻¹ with monochromatic CuKα radiation (MAC Sience, MXP18) at 30 kV and 200 mA. The morphology and particle size distribution of 1-D CeNR was determined by FE-SEM (Hitachi, S-4700 Type II) with a resolution of 0.1 nm. Nitrogen adsorption isotherms were measured at 77 K with ASAP2020 (Micromeritics Surface Area and Porosity Analyzer). The pore size distribution was determined by the method of Barrett, Joyner, and Halenda (BJH method). The XANES/EXAFS spectra were collected at the beamlines of 16A1 (Tender X-ray Absorption) at the NSRRC of Taiwan. The electron storage ring was operated with energy of 1.5 GeV and a current of 100–200 mA. The double crystal monochromator (DCM) was employed at beamline selected X-rays with energy resolving power (E/ΔE) higher than 7000 and sufficient for most XAS measurements. Data were collected in fluorescence or transmission mode with a Lytle detector (Lytle, 1999) in the regions of the Ce(5723 eV) L_{III}-edge at room temperature and analyzed with Athena. One-dimensional ceria nanorod was tested by adding the solid directly to 100 mL of metal ion solution in a 125 mL HDPE bottle. Rate constants of kinetics study were determined by adding 1 gm of CeNR to 500 mL $K_2Cr_2O_7$ (Merck) solution at room temperature (ca. 25 °C). Liquid samples were taken by a syringe every 5 min for about one hour and filtered through a 0.22 μm PVDF syringe filter (Acrodisc). The concentrations of Cr ions of the samples were further characterized by ICP/AES (Jobin Yvon Model JY32/38), AA (GBC Model 908).

3. Results and Discussion

Representative, TEM and FE-SEM micrographs of annealed ceria rod shape sample were obtained with widths of 20–40 nm in diameter and 200–300 nm in length as shown in figure 1.
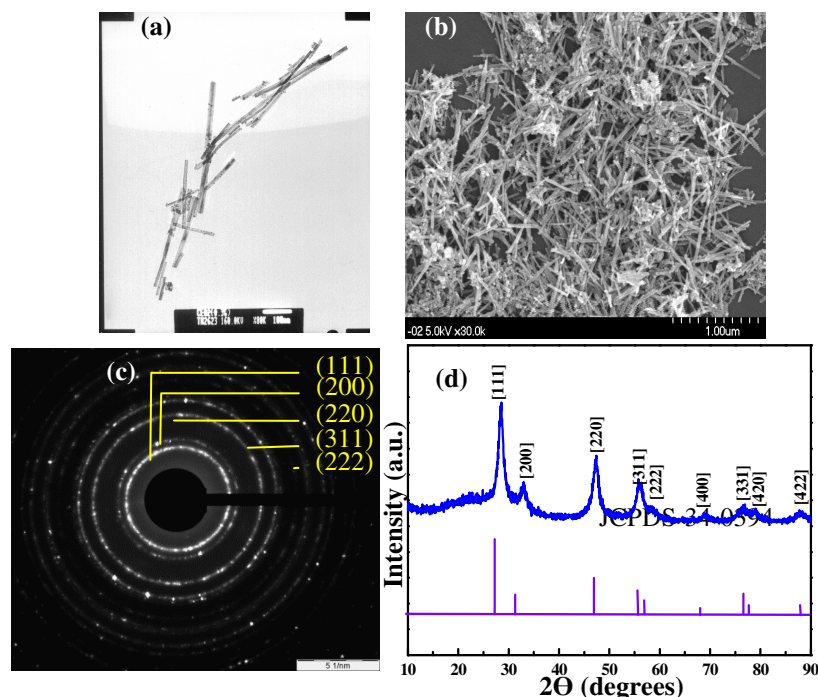

Figure 1. Microphotograph (a) TEM, (b) FE-SEM, (c) ED and (d) XRD of the ceria nanorod synthesized using hydrothermal method at 100 °C for 24 h with further calcination at 300 °C for 3 h.

The continuous ring type electron diffraction (ED) pattern in figure 1(c) confirms the polycrystalline nature of the CeNR and its face-centered cubic crystal structure. The XRD pattern of ceria nanorod is confirmed the

EESE-2013 is organised by International Society for Commerce, Industry & Engineering.

typical pattern of cubic fluorite-typed structure in figure 1(d). The average size of the crystalline ceria calculates as based on the Scherrer formula was ~8 nm with the the feature peak appears at 28.55°, in correspondence with the orientation (111) plane of CeNR structure. The BET specific surface area and pore volume of commercial ceria nanomaterials and calcined CeNR were 6 and 78 m^2g^{-1}, respectively. CeNR provided a large surface area and porous structures as compared with the different dimensional of ceria nanomaterials as shown in Table 1, so that many active sites would be useful for the Cr(VI) contaminated waste water application.

Table 1: Cr(VI) adsorption capacities of ceria adsorbents

Adsorbent	BET surface area (m^2g^{-1})	Maximum removal capacitiy ($mg\ g^{-1}$)	Size (nm)	pH
Ceria microspheres	65.0	6.76	50-100	7
3D flowerlike	34.1	5.90	4000-6000	3
Ceria nanorod	74.0	11.60	100-200	7

* Pre-adjustment of the pH value is no long necessary (Xiao, 2009).

Generally, Ce L_{III}-edge EXAFS spectroscopy can provide the information on the atomic arrangement of sorbents in terms of bond distance, coordination number, and kind of neighbors (Fernandez-García, 2002; Le Normand, 1988; Zhang, 2004). The XANES spectra for trivalent CeCl$_3$, tetravalent commercial ceria and CeNR are presented in figure 2. Trivalent CeCl$_3$ is consisted with the strongest peak at about 5724.57 eV (figure 2(a)), due to the dipole-allowed transition of Ce$2p$ to Ce $4f^1 5d$ final states and represented the 1-D CeNR (figure 2(c)) doesn't match with the CeCl$_3$ standard peak. In where, ceria nanostructure has consisted with mixed valence state at the Ce-L_{III} edge in figure 2(b) and 2(c). The four observed peaks in the Ce L_{III} edge XANES have been reported (Fernandez-García, 2002; Le Normand, 1988; Zhang, 2004). All samples have exhibited a double well known white line characteristic of double cerium ground state as $4f^0$ and $4f^1$ in agreement with the previous works (Zhang, 2004). The L_{III}-edge positions of commercial ceria and CeNR are 5716.5, 5717.64, and 5719.07 eV, respectively and are exhibited two clear peaks at 5727.5 ± 0.1 eV and 5737.4 ± 0.3 eV, respectively (Fernandez-García, 2002; Le Normand, 1988; Shahin, 2004; Zhang, 2004). A significant change in the height of the jump at the white line was observed in the 1-D CeNR samples. The change could be as a result of variation in the morphology of the samples (Shahin, 2004). It is found that the L_{III}-edge points of all the samples are consisted with the hybridization of $4f$ to $5d$ electronic state and as consisted with the electronic hole in $2p$ shell, where, $\dot{p}$ represents, as the electronic hole. The Ce $5d$ states are split in the cubic crystal field of the oxygen, resulting in the low-energy shoulder. A peak in the pre-edge region at 5717.3±0.2 eV with lower photon energy can be obtained by curve fitting (Fernandez-García, 2002).
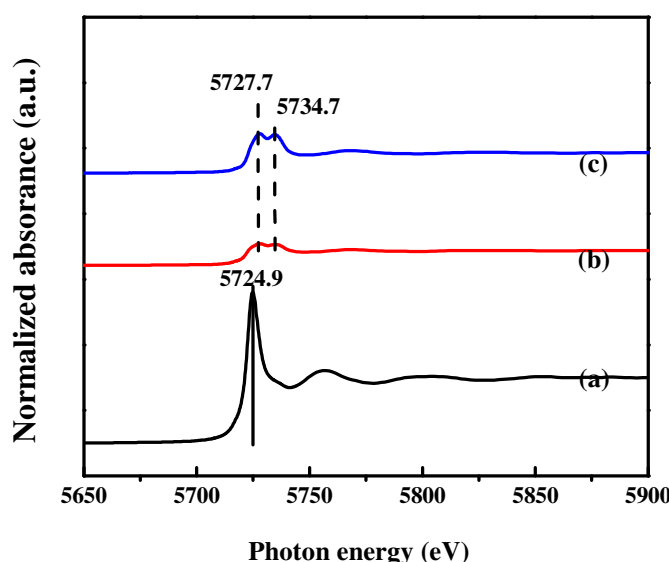

Figure 2. XANES spectra of (a) CeCl$_3$ standard, (b) commercial ceria powder, and (c) ceria nanorod synthesized at 100 °C for 24 h with further calcination at 300 °C for 3 h.

The pre-edge region is assisted with the dipole-forbidden $2p_{3/2} \rightarrow 4f$ transition, thus affects the $5d \rightarrow 4f$ transition state to form $4f^1 5d^1$ and $4f^0 5d^1$ electronic configuration (Shahin, 2004). In addition, peak position at 5723.64 ± 0.1 eV has been influenced with the $2p_{3/2} \rightarrow 4f$ transition too and formed $2p4f^1 5d^0 \rightarrow 2\dot{p}^5 4f^1 5d^1$ transition (Bianconi, 1987). The variation of the particle morphology altered particle nucleation. Thus around ~2eV shift of binding

Journal of Energy Technologies and Policy   www.iiste.org
ISSN 2224-3232 (Paper)   ISSN 2225-0573 (Online)
Vol.3, No.11, 2013 – Special Issue for International Conference on Energy, Environment and Sustainable Economy (EESE 2013)

energy has been occurred for CeNR from commercial ceria nanostructure. The intensities of the first peak of a white line at 5727.5 $\pm$ 0.1 eV were due to the $2p4f^15d^0 \rightarrow 2p^54f^15d^1$ transition, whereas the second peak at 5737.4 $\pm$ 0.3 eV were due to a $2p4f^05d^0 \rightarrow 2p^64f^05d^1$ transition (Shahin, 2004). In addition, fluorite structure of 1-D CeNR Ce has 8 and 12 neighboring atoms in the first and second coordination shell corresponding to Ce-O and Ce-Ce correlations (Fernandez-García, 2002).

It can be seen that Ce-O bond distance of 2.4 Å and the coordination number of 6.87 for the CeNR samples were attenuated with the cerium and affordable existent with trivalent cerium oxide as shown in Table 2. Two approaches were taken according to the fitting of the crystallographic data. In the first case, the coordination number was held at the crystallographic values with the radial distance and Debye–Waller's factors were varied. Ceria nanoparticles have consisted with a bond length of 2.3 Å and a coordination number of 4.53. The apparent shortening of the Ce-O bond length probably was caused by the random motion of the surface atom on Ce particles instead of a true shortening of the bond distance. Moreover, bond distance of CeNR is approached to trivalent cerium oxide and is larger than commercial ceria. That represent CeNR has higher content of trivalent cerium oxide and that can effectively take to participate for Cr(VI) contaminated waste-water treatment.

Table 2. Structural parameters of ceria analyzed by EXAFS

Bonding pair		CN^a	$R^b(\text{Å})$	$\Delta\sigma^{2c}(\text{Å}^2)$
CeCl$_3$ standard	(Ce-O)	4.53	2.32	0.00099
Commercial ceria	(Ce-O)	4.53	2.32	0.00086
1-D ceria- nanorod	(Ce-O)	6.87	2.41	0.00329

The effect of contact time on the amount of Cr(VI) adsorbed onto CeNR was measured at the different initial concentration (20 to 80 ppm) in the presence of 1g of the one-dimensional ceria was added to 500 mL Cr(VI) solution at room temperature as shown in figure 3. The adsorption rate was rather fast and Cr(VI) could be removed after 160 min. This value is fairly higher than the bulk ceria to remove Cr(VI) due to the reflect of higher surface area and oxidation state enhance the adsorption affinity of 1-D CeNR and the Cr(VI) species by ion-exchange (Di, 2006; Jinhua, 2010; Xiao, 2009).
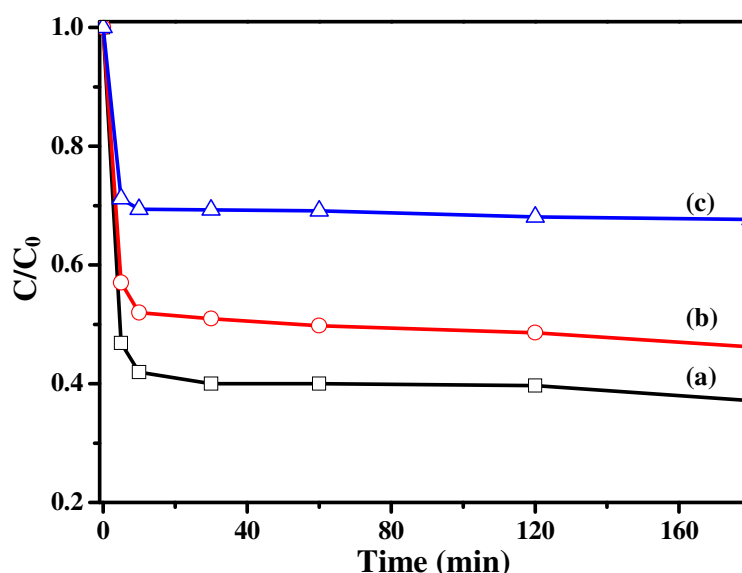

Figure 3. Adsorption rate of Cr with different concentration (a) 20, (b) 40, and (c) 80 ppm respectively. CeNR sample of 1g and 500 mL of aqueous solution have been taken at room temperature for adsorption analysis.

A simple kinetic analysis is performed with the aid of pseudo-second-order equation. In this equation, the value of the rate constant k can be calculated in the form:

$$\frac{dq_t}{dt} = k(q_e - q_t)^2 \tag{1}$$

Where q_e and q_t are the amount of Cr(VI) adsorbed per unit mass (mg.g^{-1}) of the adsorbent at equilibrium and time t (min), respectively. After definite integration is applying the initial conditions $q_t = 0$ at $t = 0$ and $q_t = q_t$ at $t = t$, Eq. (1) becomes

$$\frac{t}{q_t} = \frac{1}{kq_e^2} + \frac{1}{q_e}t .$$

(2)

Nonlinear regressions using a least-squares fitting program (Origin 7.0, OriginLab Corp. Northampton, MA) were conducted to acquire the best estimate of all constants for all the models. The fitting plots using pseudo-second-order equation is shown in figure 4. The kinetic parameters acquired from fitting results are summarized in Table 3.
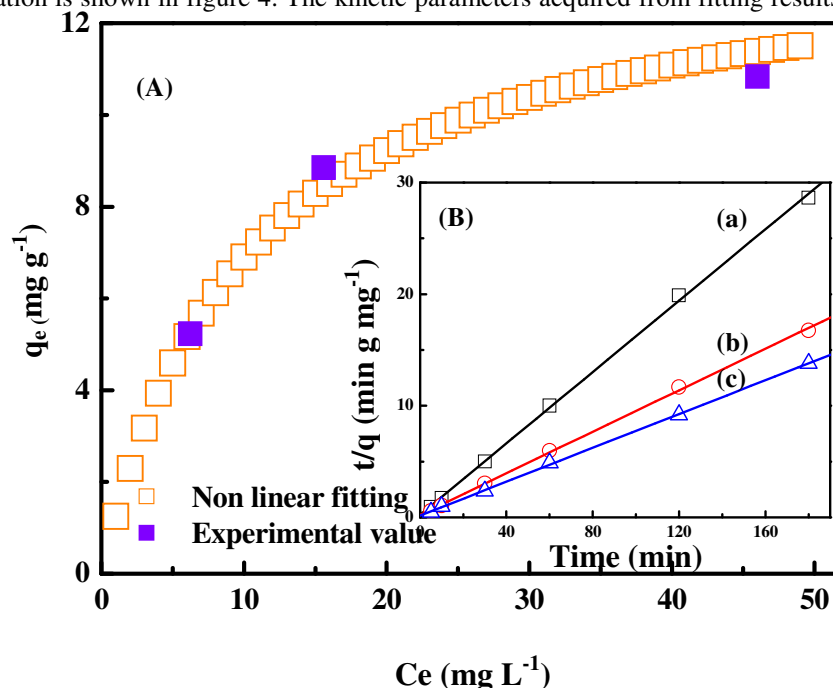

Figure 4. (A) Adsorption isotherms of Cr(VI) and (B) pseudo-second order diffusion kinetic models for Cr with different concentration of (a) 20, (b) 40, and (c) 80 ppm in the 1 g CeNR 500 mL solution at room temperature.

Table 3. Kinetic parameters of chromium contaminants

Concentration (ppm)	Rate constant, K (g.min^{-1} mg^{-1})	q_e (mg.g^{-1})	Regression, R^2
20	0.10	6.26	0.9991
40	0.03	10.75	0.9993
80	0.05	12.97	0.9997

The maximum adsorption capacity (figure 4(a)) can be observed as 11.6 mg g^{-1} and is consisted with higher adsorption of Cr(VI) as compared with bulk ceria as shown in Table 1. In addition, Linear plots of the t/q_t versus t with linear regression coefficients is higher than 0.999 indicated the applicability of this kinetic equation and the pseudo-second nature of the adsorption process for Cr(VI) onto CeNR and is closer to chemisorptions as confirmed in the figure 4(b) and Table 3. This result suggested that higher BET surface area and oxygen vacancy as revealed by XANES/EXAFS analysis from one-dimensional CeNR is facilitate the diffusion and adsorption of Cr(VI) contaminated waste-water treatment (Xiao, 2009).

Conclusions

Morphology and structure of the ceria enhance the reactivity of the Cr(VI) from waste water enormously. The FE-SEM photographs of 1-D CeNR catalysts used for the remediation of Cr-contaminated waste water indicated ceria were nearly rod shape particles, which were 20–40 nm in diameter and 200–300 nm in length, respectively. On the contrary, higher surface area is readily involved to the enhancement of Cr-contaminated wastewater remediation. By XANES/EXAFS, it was found that mainly 1-D ceria possess higher oxidation states than commercial ceria nanoparticle and thus may involve in the wastewater treatment. The high reaction rates and

significant removal of toxic Cr contaminants are suggested that the nanophase 1-D CeNR catalysts might be a suitable material for *in- situ* remediation of Cr(VI) or Cr(III)-contaminated groundwater or waste streams.

Acknowledgements

References

Bianconi, A., Marcelli, A., Dexpert, H., Karnatak, R., Kotani, A., Jo, T.,Petiau, J. (1987). Specific intermediate-valence state of insulating 4f compounds detected by L_3 x-ray absorption. *Physical Review B 35*(2), 806.

Chowdhury, S.,Lin, K.-S. (2012). Characterization and surface reactivity analyses of ceria nanorod catalyst for methanol interaction. *Materials Chemistry and Physics 133*(1), 163–169.

Chowdhury, S.,Lin, K. S. (2011). Synthesis and characterization of 1D ceria nanomaterials for CO oxidation and steam reforming of methanol. *Journal of Nanomaterials 2011*.

Di, Z.-C., Ding, J., Peng, X.-J., Li, Y.-H., Luan, Z.-K.,Liang, J. (2006). Chromium adsorption by aligned carbon nanotubes supported ceria nanoparticles. *Chemosphere 62*(5), 861–865.

Fernandez-García, M. (2002). XANES analysis of catalytic systems under reaction conditions. *Catalysis Reviews-Science and Engineering 44*(1), 59–121.

Jinhua, W., Xiang, Z., Bing, Z., Yafei, Z., Rui, Z., Jindun, L.,Rongfeng, C. (2010). Rapid adsorption of Cr (VI) on modified halloysite nanotubes. *Desalination 259*(1–3), 22–28.

Le Normand, F., Hilaire, L., Kili, K., Krill, G.,Maire, G. (1988). Oxidation state of cerium in cerium-based catalysts investigated by spectroscopic probes. *The Journal of Physical Chemistry 92*(9), 2561–2568.

Lin, K. S.,Chowdhury, S. (2010). Synthesis, characterization, and application of 1-D cerium oxide nanomaterials: a review. *International Journal of Molecular Science 11*(9), 3226–32251.

Lytle, F. W. (1999). The EXAFS family tree: A personal history of the development of extended X-ray absorption fine structure. *Journal of Synchrotron Radiation 6*(3), 123–134.

Ponder, S. M., Darab, J. G.,Mallouk, T. E. (2000). Remediation of Cr(VI) and Pb(II) Aqueous Solutions Using Supported, Nanoscale Zero-valent Iron. *Environmental Science & Technology 34*(12), 2564–2569.

Qi, R. J., Zhu, Y. J., Cheng, G. F.,Huang, Y. H. (2005). Sonochemical synthesis of single-crystalline $CeOHCO_3$ rods and their thermal conversion to CeO_2 rods. *Nanotechnology 16*(11), 2502–2506.

Shahin, A. M., Grandjean, F., Long, G. J.,Schuman, T. P. (2004). Cerium LIII-Edge XAS Investigation of the Structure of Crystalline and Amorphous Cerium Oxides. *Chemistry of Materials 17*(2), 315–321.

Wang, X., Wang, J., Chang, L., Ding, Q., Liu, H.,Jiang, X. (2012). Tunable synthesis of novel 3D CuI hierarchical architectures and their excellent Cr(VI) removal capabilities. *RSC Advances 2*(32), 12315–12321.

Xiao, H., Ai, Z.,Zhang, L. (2009). Nonaqueous sol−gel synthesized hierarchical CeO_2 nanocrystal microspheres as novel adsorbents for wastewater treatment. *Journal of Physical Chemistry C 113*(38), 16625–16630.

Zhang, D., Ni, X., Zheng, H., Zhang, X.,Song, J. (2006). Fabrication of rod-like CeO_2: Characterization, optical and electrochemical properties. *Solid State Sciences 8*(11), 1290−1293.

Zhang, F., Wang, P., Koberstein, J., Khalid, S.,Chan, S.-W. (2004). Cerium oxidation state in ceria nanoparticles studied with X-ray photoelectron spectroscopy and absorption near edge spectroscopy. *Surface Science 563*(1-3), 74–82.